Contribution of Strong Discontinuities to the Power Spectrum of the Solar Wind

Joseph E. Borovsky
Los Alamos National Laboratory, Los Alamos, New Mexico, 87545, USA
(Received 25 February 2010; published 8 September 2010)

Eight and a half years of magnetic field measurements (2^{22} samples) from the ACE spacecraft in the solar wind at 1 A.U. are analyzed. Strong (large-rotation-angle) discontinuities in the solar wind are collected and measured. An artificial time series is created that preserves the timing and amplitudes of the discontinuities. The power spectral density of the discontinuity series is calculated and compared with the power spectral density of the solar-wind magnetic field. The strong discontinuities produce a power-law spectrum in the ''inertial subrange'' with a spectral index near the Kolmogorov $-5/3$ index. The discontinuity spectrum contains about half of the power of the full solar-wind magnetic field over this ''inertial subrange.'' Warnings are issued about the significant contribution of discontinuities to the spectrum of the solar wind, complicating interpretation of spectral power and spectral indices.

DOI: 10.1103/PhysRevLett.105.111102 PACS numbers: 96.50.Tf, 52.35.Ra, 96.50.Bh, 96.50.Ry

The objective of this Letter is to demonstrate that discontinuities in the solar-wind plasma have an unignorable impact on the magnetic energy spectrum.

Solar-wind discontinuities are characterized by large rapid changes in the properties of the plasma. Typically they are identified via changes in the direction of the solar-wind magnetic field. In Fig. 1 the distribution of magnetic-field angular direction changes $\Delta\theta$ over 128-s time intervals is plotted for 11 years of measurements by the ACE spacecraft at 1 A.U. The distribution contains two populations (cf. [1]): a population of small changes that is well fit by a steep exponential and a population of large changes that is well fit by a shallower exponential. The population of large changes has been identified as strong discontinuities in the solar wind and the smaller fluctuations have been identified with the MHD turbulence [1]. The population of discontinuities extends to below $\Delta\theta = 45°$, but with field measurements alone it cannot be separated from the population of smaller fluctuations; to view the discontinuity population at small $\Delta\theta$ values see Fig. 17 of Borovsky [2] where ion-specific-entropy changes and field-strength changes were used to identify discontinuities. Strong discontinuities have flow-velocity jumps δv in addition to field rotations $\Delta\theta$. For the population with $\Delta\theta > 45°$, the δv are on the order of the Alfven speed v_A and the ion-thermal velocity v_{Ti}: $\delta v/v_A = 0.77 \pm 0.54$ and $\delta v/v_{Ti} = 1.09 \pm 0.70$. Often strong discontinuities show sudden changes in the properties of the solar-wind plasma [1–3] and 66% show internal depressions of the magnetic-field strength.

Early surveys of solar-wind discontinuities identified the majority as rotational discontinuities (Alfven waves) [4–8], but more-modern surveys identify the majority as tangential discontinuities (plasma boundaries) [9–13]. The time interval between the passages of subsequent strong (large-angle) discontinuities varies from seconds to hours (e.g., [1,3,14]). Tangential discontinuities in the solar wind are highly Alfvenic [6,15,16] and strong discontinuities make a significant contribution to the Alfvenicity of the solar wind [17]. Thicknesses of strong discontinuities vary from 10^3–10^5 km [14,18].

One interpretation of the strong discontinuities is that they are the walls of a filamentary structure of the solar wind [1,4,17,19–31]; another is that they are boundaries in a discontinuous solar-wind plasma [3,18]. Some strong discontinuities are fossils from the birth of the solar wind [1,3,25,26,32]. Some could be formed away from the Sun by relaxation of the solar-wind magnetic-field structure [33–36]. Nontangential discontinuities could be formed away from the Sun by steepening of large-amplitude Alfven waves [37,38] and discontinuities can be formed

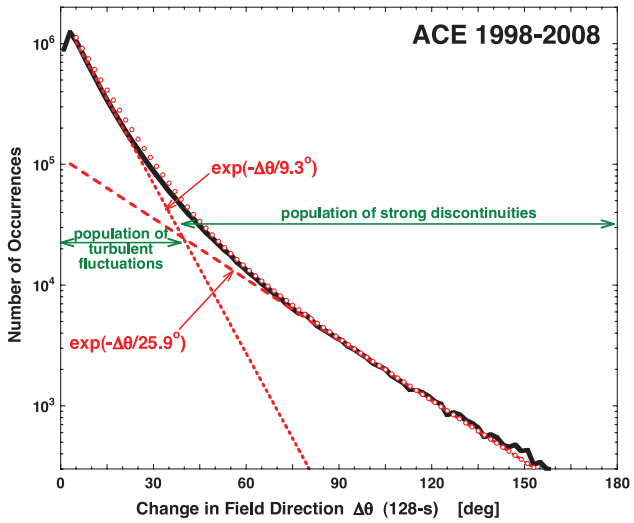

FIG. 1 (color). Using 11 years of measurements, the angular change $\Delta\theta$ in the direction of the solar-wind magnetic field every 128 seconds is binned (black curve). The distribution is fit by two exponentials (dashed red curves) and the sum of the two exponentials is plotted as the red points.

from steepening of Alfven waves in the presence of collisionless dissipation [39,40]. Current sheets can also form as a consequence of the cascade of MHD turbulence to kinetic scales [41–43], which would produce small-angle discontinuities with thickness on the order of the ion inertial length or ion gyroradius (tens of kilometers) [44,45].

Conventional wisdom has it that a time series of discontinuities produces an f^{-2} energy spectrum [46,47]. The magnetic energy spectrum of the solar wind is usually characterized by an approximately $f^{-5/3}$ (Kolmogorov [48]) or $f^{-3/2}$ (Kraichnan [49]) spectrum in the inertial subrange (few hours to tens of seconds) [50–52]. At lower frequencies the magnetic energy spectrum is flatter, being interpreted as unevolved structure from the Sun [53,54]. Siscoe *et al.* [14] and Sari and Ness [55] warned that discontinuities could have a significant impact on the energy spectra of the solar wind. Siscoe *et al.* pointed out that discontinuities could produce spectral indices shallower than f^{-2} for limited ranges of frequency. It will be demonstrated below that discontinuities can produce shallower than f^{-2} spectra over broad frequency intervals.

To demonstrate this we will collect and measure the discontinuities in the solar wind and create an artificial time series representing the properties of these discontinuities. The energy spectrum of that collection of discontinuities will then be compared with the energy spectrum of the solar-wind magnetic field.

The data utilized is 64-sec averages of the vector magnetic field measured [56] from the ACE spacecraft at 1 A.U.; 8.51 years of data is used from 1998-2006, comprising $2^{22} = 4\,194\,304$ measurements at a 64-sec cadence. No attempt is made to remove shocks, ejecta, etc. The radial-tangential-normal coordinate system [57] is employed.

In the ACE magnetic-field time series, a strong discontinuity is marked whenever $\Delta\theta > 45°$ in 128 s (see Fig. 1), and the time and vector amplitude $(\Delta B_r, \Delta B_t, \Delta B_n)$ of each discontinuity is recorded. (See Li [31,58] for a confirmation of the robustness of this method for identifying discontinuities.) 160 465 discontinuities are collected; the mean time between subsequent discontinuities is ~28 min. To create a time series $\underline{D}(t) = (D_r(t), D_t(t), D_n(t))$ of vectors that contains the signal of the discontinuities a function is created that is constant until a discontinuity occurs [with amplitude $(\Delta B_r, \Delta B_t, \Delta B_n)$] at which time the value of vector $\underline{D}(t)$ is changed from the "old" value to a "new" value given by $D_{r\mathrm{new}} = D_{r\mathrm{old}} - |\Delta B_r| D_{r\mathrm{old}}/|D_{r\mathrm{old}}|$, $D_{t\mathrm{new}} = D_{t\mathrm{old}} - |\Delta B_t| D_{t\mathrm{old}}/|D_{t\mathrm{old}}|$, and $D_{n\mathrm{new}} = D_{n\mathrm{old}} - |\Delta B_n| D_{n\mathrm{old}}/|D_{n\mathrm{old}}|$. Hence if D_r is positive, the ΔB_r change in D_r is taken to be negative, and if D_r is negative the change is positive. The same for D_t and D_n. This prevents the function $\underline{D}(t)$ from drifting too far from (0,0,0), preserving the timing and step amplitudes of the discontinuities but eliminating the envelope function of the magnetic-field values. $\underline{D}(t)$ is shown in Fig. 2; the components of the magnetic field $\underline{B}(t)$ (top panel) and the components of the resulting discontinuity function $\underline{D}(t)$ (bottom panel) are plotted for 12 hours. The mean directional change of the field at a strong discontinuity is 68°; the mean 128-s direction change for the fluctuations that have been removed between the discontinuities is 10°.

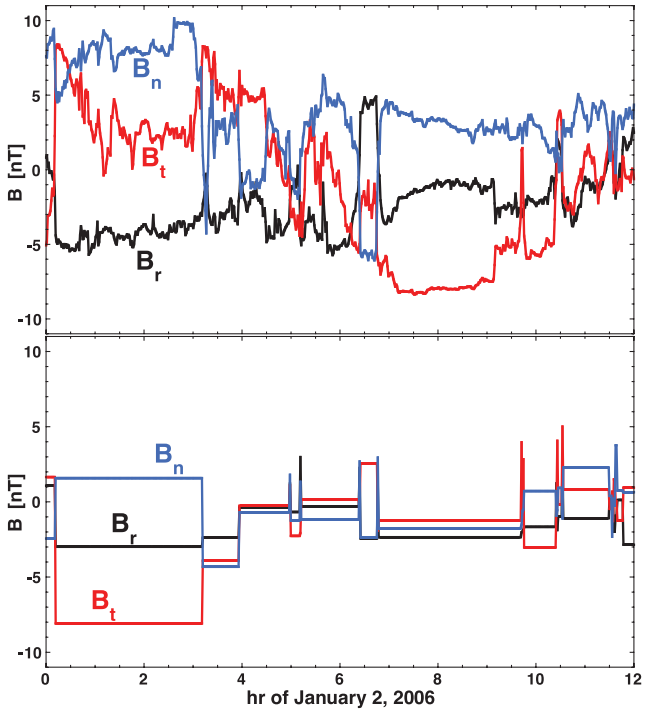

FIG. 2 (color). The magnetic-field time series $(B_r(t), B_t(t), B_n(t))$ is plotted for 12 hours in the top panel and the resulting discontinuity time series $(D_r(t), D_t(t), D_n(t))$ is plotted in the bottom panel.

The time series $\underline{D}(t)$ created from the strong $(\Delta\theta > 45°)$ discontinuities is Fourier transformed using fast-Fourier-transform algorithm (FFT) techniques [59]. Denoting the Fourier transform of $(D_r(t), D_t(t), D_n(t))$ as $(\mathcal{D}_r(f), \mathcal{D}_t(f), \mathcal{D}_n(f))$, the power spectral density $P_{\mathrm{disc}}(f)$ of $\underline{D}(t)$ is $P_{\mathrm{disc}} = \mathcal{D}_r^2 + \mathcal{D}_t^2 + \mathcal{D}_n^2$.

In Fig. 3 the power spectral density of the discontinuities for 8.5 years of ACE data is plotted (black) from $f = 10^{-8}$ s^{-1} to $f = f_N/4$, where $f_N = 7.81 \times 10^{-3}$ s^{-1} is the Nyquist frequency. A 21-point running average is plotted as the blue points and a 300-point average as the yellow. Notice that the discontinuity energy spectrum has a power-law form from $f \sim 1 \times 10^{-4}$ s^{-1} to $f_N/4$. This corresponds to periods from 2.8 hr to 512 s, which comprises the lower-frequency portion of the "inertial subrange" of the solar wind. The purple line in Fig. 3 is a power-law fit to the black points over the 1×10^{-4}–1.86×10^{-3} s^{-1} range: that fit is

$$P_{\mathrm{disc}} = 5.6 \times 10^{-3} f^{-1.68} \qquad (1)$$

in units of nT^2 Hz^{-1} for the collection of strong discontinuities.

For comparison, the power spectral density $P_{\mathrm{mag}} = \mathcal{B}_r^2 + \mathcal{B}_t^2 + \mathcal{B}_n^2$ of the solar-wind magnetic-field time series $\underline{B}(t)$ is calculated for the same time interval.

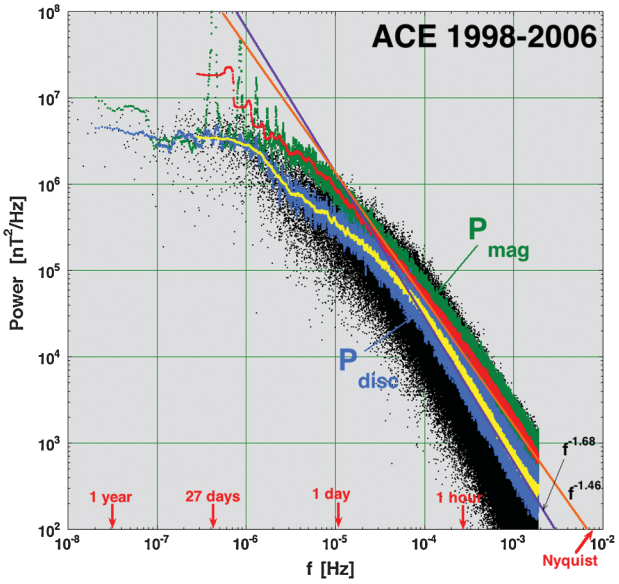

FIG. 3 (color). For 8.5 years of measurements of the magnetic field at 1 A.U., the power spectral density of the discontinuities $P_{\rm disc}$ is plotted (black points = no averaging; blue = 21-point running average; yellow = 300-point running average) and the power spectral density of the magnetic field $P_{\rm mag}$ is plotted (green points = 21-point running average; red = 300-point running average). Fits to the unaveraged data appear as the purple line and the orange line.

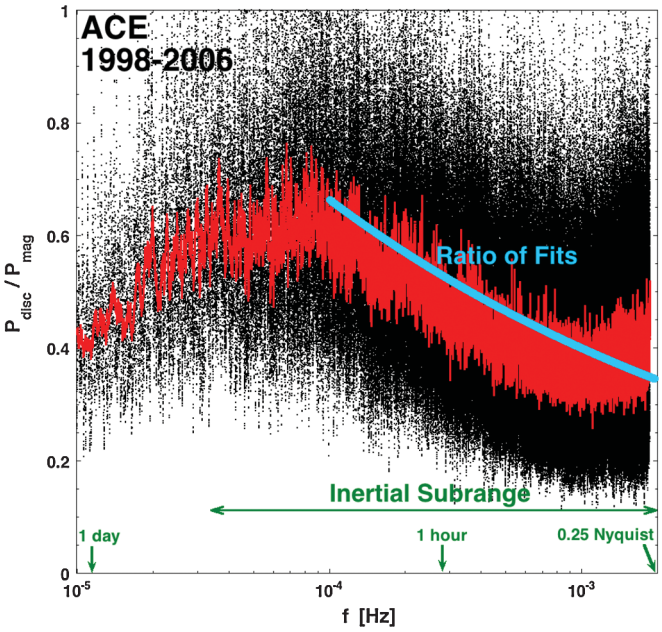

FIG. 4 (color). The ratio of the power spectral density of the discontinuities $P_{\rm disc}$ to that of the magnetic field $P_{\rm disc}$ is plotted. The black points are ratios of 21-point running averages of $P_{\rm disc}$ and $P_{\rm disc}$, the red points are from ratios of 300-point running averages, and the blue is the ratio of the power-law fits to $P_{\rm disc}$ and $P_{\rm disc}$.

In Fig. 3 the 21-point running average of this is plotted in green and the 300-point average in red. Over the inertial subrange note the similarity in spectral shape of the red (full magnetic) and yellow (strong-discontinuity) curves. For $1 \times 10^{-4}\ \mathrm{s}^{-1} < f < 1.86 \times 10^{-3}\ \mathrm{s}^{-1}$ the magnetic energy spectrum is fit (orange line) as

$$P_{\rm mag} = 6.4 \times 10^{-2} f^{-1.46} \qquad (2)$$

in $\mathrm{nT}^2\,\mathrm{Hz}^{-1}$ (see also [52]). This power-law form of the magnetic energy spectrum has been taken to be evidence of a turbulent cascade in the solar wind [60–63]. Here it is found that the spectral index of the magnetic field (-1.46) is very similar to the spectral index of the strong discontinuities (-1.68).

In Fig. 4 the ratio of the power spectral density of the strong discontinuities $P_{\rm disc}$ to that of the magnetic field $P_{\rm mag}$ is plotted as a function of frequency. This ratio is calculated from 21-point running averages (black points) and 300-point running averages (red points); also plotted (blue) is the ratio of the power-law fits (1) and (2). As seen, in the inertial subrange the strong discontinuities contain about half of the spectral power of the solar wind. Note that only strong discontinuities were used; weaker discontinuities, which are more difficult to locate, were not collected. Had the weaker discontinuities been included in the analysis, the fraction of the power spectral density attributable to discontinuities would be even larger.

Note that a somewhat different study was performed [47] wherein jumps in the 1-hr-averaged time series of solar-wind $|B|$ measurements were collected and an artificial time series was created from those jumps. Strong jumps in $|B|$ occur on a ~10-day time scale. At periods shorter than 10 days the energy spectra of the jump time series was found to be a power law steeper than f^{-2}, which is as expected for time scales shorter than interjump time scales. In the present study time scales comparable to interjump time scales are of interest, wherein the spectral slopes are shallower than f^{-2} (cf. Ref. [64]).

Summarizing the findings for the solar wind at 1 A.U.: (1) Strong solar-wind discontinuities can give rise to power-law spectra with spectral indices similar to the Kolmogorov $-5/3$ and Kraichnan $-3/2$ indices. (2) Strong discontinuities dominate, or at least strongly contribute to, the spectrum in the inertial subrange. Some strong discontinuities in the solar wind can be nonevolving fossil structure from the Sun (Refs. [1,2,18,25]).

The implication of these findings is the following: Any interpretation of the dynamics or evolution of the solar wind should account for the contribution of strong discontinuities to the measurements and should be based on the properties of a plasma containing strong discontinuities and plasma boundaries.

In general, turbulence interpretations of the dynamics and evolution of the solar-wind plasma do not account for the large contribution of strong discontinuities to the power spectra (see Refs. [40,65] for exceptions). Such interpretations appear deficient.

The author thanks Mick Denton for his help. This research was supported by the NASA Heliospheric SR&T

Program, the NASA Heliospheric Guest-Investigator Program, by the NSF SHINE Program, and by the LDRD Program at Los Alamos National Laboratory.

[1] J. E. Borovsky, J. Geophys. Res. **113**, A08110 (2008).
[2] J. E. Borovsky, "On the Variations of the Solar-Wind Magnetic Field about the Parker-Spiral Direction," J. Geophys. Res. (to be published).
[3] L. F. Burlaga, Sol. Phys. **7**, 54 (1969).
[4] F. Mariani *et al.*, J. Geophys. Res. **78**, 8011 (1973).
[5] F. Mariani, B. Bavassano, and U. Villante, Sol. Phys. **83**, 349 (1983).
[6] M. Neugebauer *et al.*, J. Geophys. Res. **89**, 5395 (1984).
[7] M. Neugebauer and C. J. Alexander, J. Geophys. Res. **96**, 9409 (1991).
[8] B. T. Tsurutani and C. M. Ho, Rev. Geophys. **37**, 517 (1999).
[9] T. S. Horbury *et al.*, Geophys. Res. Lett. **28**, 677 (2001).
[10] T. Knetter *et al.*, Adv. Space Res. **32**, 543 (2003).
[11] T. Knetter *et al.*, J. Geophys. Res. **109**, A06102 (2004).
[12] M. O. Riazantseva, G. N. Zastenker, and J. D. Richardson, Adv. Space Res. **35**, 2147 (2005).
[13] M. O. Riazantseva *et al.*, J. Geophys. Res. **110**, A12110 (2005).
[14] G. L. Siscoe *et al.*, J. Geophys. Res. **73**, 61 (1968).
[15] M. Neugebauer *et al.*, J. Geophys. Res. **91**, 13 694 (1986).
[16] M. Neugebauer, J. Geophys. Res. **90**, 6627 (1985).
[17] J. E. Borovsky and M. H. Denton, "Solar-Wind Turbulence and Shear: A Superposed-Epoch Analysis of Corotating Interaction Regions at 1 A.U.," J. Geophys. Res. (to be published).
[18] J. E. Borovsky, Phys. Plasmas **13**, 056505 (2006).
[19] E. N. Parker, *Interplanetary Dynamical Processes* (Wiley Interscience, New York, 1963), Ch. XIV.
[20] E. N. Parker, Astrophys. J. **139**, 690 (1964).
[21] N. F. Ness, C. S. Scearce, and S. Cantarano, J. Geophys. Res. **71**, 3305 (1966).
[22] K. G. McCracken and N. F. Ness, J. Geophys. Res. **71**, 3315 (1966).
[23] W. C. Bartley *et al.*, J. Geophys. Res. **71**, 3297 (1966).
[24] K. M. Thieme, E. Marsch, and R. Schwenn, in *Proceedings of the Sixth International Solar Wind Conference*, edited by V. J. Pizzo, T. Holzer, and D. G. Sime (National Center for Atmospheric Research, Boulder, 1988), pg. 317, Technical Note NCAR/TN-306 +Proc.
[25] K. M. Thieme, R. Schwenn, and E. Marsch, Adv. Space Res. **9**, 127 (1989).
[26] K. M. Thieme, E. Marsch, and R. Schwenn, Ann. Geophys. **8**, 713 (1990).
[27] C.-Y. Tu and E. Marsch, J. Geophys. Res. **95**, 4337 (1990).
[28] C.-Y. Tu and E. Marsch, J. Geophys. Res. **98**, 1257 (1993).
[29] E. Marsch, in *Physics of the Inner Heliosphere II*, edited by R. Schwenn and E. Marsch (Springer-Verlag, Berlin, 1991), Sect. 10.2.2.
[30] R. Bruno *et al.*, Planet. Space Sci. **49**, 1201 (2001).
[31] B. Li, AIP Conf. Proc. **932**, 26 (2007).
[32] L. F. Burlaga, Sol. Phys. **4**, 67 (1968).
[33] E. N. Parker, *Spontaneous Current Sheets in Magnetic Fields* (Oxford University Press, New York, 1994).
[34] E. N. Parker, Phys. Plasmas **11**, 2328 (2004).
[35] E. R. Priest, J. F. Heyvaerts, and A. N. Title, Astrophys. J. **576**, 533 (2002).
[36] R. M. Close, J. F. Heyvaerts, and E. R. Priest, Sol. Phys. **225**, 267 (2004).
[37] F. Malara, L. Primavera, and P. Veltri, J. Geophys. Res. **101**, 21597 (1996).
[38] B. J. Vasquez and J. V. Hollweg, J. Geophys. Res. **104**, 4681 (1999).
[39] M. V. Medvedev *et al.*, Phys. Rev. Lett. **78**, 4934 (1997).
[40] M. V. Medvedev, Phys. Plasmas **6**, 2191 (1999).
[41] D. Biskamp and H. Welter, Phys. Fluids B **1**, 1964 (1989).
[42] P. Dmitruk, W. H. Matthaeus, and N. Seenu, Astrophys. J. **617**, 667 (2004).
[43] A. Greco *et al.*, Geophys. Res. Lett. **35**, L19111 (2008).
[44] B. J. Vasquez *et al.*, J. Geophys. Res. **112**, A11102 (2007).
[45] M. Neugebauer and J. Giacalone, AIP Conf. Proc. **1216**, 194 (2010).
[46] D. C. Champeney, *Fourier Transforms and their Physical Applications* (Academic Press, London, 1973).
[47] D. A. Roberts and M. L. Goldstein, J. Geophys. Res. **92**, 10 105 (1987).
[48] U. Frisch, *Turbulence* (Cambridge University Press, Cambridge, 1995).
[49] R. H. Kraichnan, Phys. Fluids **8**, 1385 (1965).
[50] W. H. Matthaeus and M. L. Goldstein, J. Geophys. Res. **87**, 6011 (1982).
[51] A. Mangeney, R. Grappin, and M. Velli, in *Advances in Solar System Magnetohydrodynamics*, edited by E. R. Priest and A. W. Hood (Cambridge University Press, Cambridge, 1991), pg. 327.
[52] J. J. Podesta, D. A. Roberts, and M. L. Goldstein, J. Geophys. Res. **111**, A10109 (2006).
[53] W. H. Matthaeus and M. L. Goldstein, Phys. Rev. Lett. **57**, 495 (1986); C.-Y. Tu, Z. Y. Pu, and F.-S. Wei, J. Geophys. Res. **89**, 9695 (1984).
[54] M. L. Goldstein and D. A. Roberts, Phys. Plasmas **6**, 4154 (1999).
[55] J. W. Sari and N. F. Ness, Sol. Phys. **8**, 155 (1969).
[56] C. W. Smith *et al.*, Space Sci. Rev. **86**, 613 (1998).
[57] A. Alevizos *et al.*, Sol. Phys. **186**, 401 (1999).
[58] G. Li, Astrophys. J. **672**, L65 (2008).
[59] R. K. Otnes and L. Enochson, *Digital Time Series Analysis* (Wiley, New York, 1972), Chap. 5 and 6.
[60] P. J. Coleman, Astrophys. J. **153**, 371 (1968).
[61] T. S. Horbury, M. A. Forman, and S. Oughton, Plasma Phys. Controlled Fusion **47**, B703 (2005).
[62] M. Dobrowolny, A. Mangeney, and P. L. Veltri, Phys. Rev. Lett. **45**, 144 (1980).
[63] C.-Y. Tu, Z. Y. Pu, and F.-S. Wei, J. Geophys. Res. **89**, 9695 (1984).
[64] S. B. Lowen and M. C. Teich, Phys. Rev. E **47**, 992 (1993).
[65] M. V. Medvedev and P. H. Diamond, Phys. Rev. E **56**, R2371 (1997).